Marine Structures 46 (2016) 56–77

Contents lists available at ScienceDirect

Marine Structures

journal homepage: www.elsevier.com/locate/marstruc

Numerical and experimental analysis on motion performance of new sandglass-type floating body in waves

Wen-hua Wang, Lin-lin Wang, Ya-zhen Du, Yu-xin Yao, Yi Huang*

School of Naval Architecture, Dalian University of Technology, Dalian, 116024, China

ARTICLE INFO

Article history:
Received 5 August 2015
Received in revised form 8 December 2015
Accepted 9 December 2015
Available online xxx

Keywords:
Sandglass-type floating body
Shape parameter
Heave motion performance
Engineering estimation expression
Design guideline
Cylindrical FPSO

ABSTRACT

In order to solve the performance limitations of traditional ship-type and cylindrical FPSO, this paper presents a new concept of sandglass-type FPSO. For the new sandglass-type floating model, firstly by using classic boundary element method based on wave potential theory, the effects of shape parameters on motion performance of sandglass-type model are studied. Then the wave frequency versus minimum heave motion RAO is selected as the critical design parameter to control heave motion of new floating model, and its convenient engineering estimation expression is theoretically and mathematically deduced. Furthermore, on this basis the design guideline for sandglass shape is analyzed and proposed. Next according to the information of a cylindrical FPSO, a sandglass-type floating model with the same basic function has been designed. Finally, by analyzing the numerical solution and experimental data, the numerical boundary element method and design guideline in this paper can be validated to be effective and accurate. Furthermore, it can be found that the sandglass-type design can obviously improve the hydrodynamic performance of FPSO. Thus this paper can provide an innovative engineering platform and a design proposal for the development of ocean oil and gas exploitation.

* Corresponding author.
E-mail address: huangyi@dlut.edu.cn (Y. Huang).

http://dx.doi.org/10.1016/j.marstruc.2015.12.002
0951-8339/

1. Introduction

As ocean oil and gas exploration expands towards the deep sea in harsh environments, FPSO (floating production, storage and offloading unit) has played an important part in the development mode, due to its large capacity of oil storage, multifunction, strong adaptability and convenience for maintenance and repair. In the future, FPSO will have wide and good application prospects [2,4,14].

Traditional ship-type and cylindrical FPSOs exhibit some performance shortcomings [17,19]. Firstly, the traditional ship-type floating body is extremely sensitive to the wave direction. Secondly, with the complicated environment and single point mooring system, FPSO would be usually in the oblique (beam) sea, which may result in poor heave and roll performance. Next, because the longitudinal scale is extremely large, the phenomenon of wave impact and green water is common and would damage the deck structure. Furthermore, the vane effect will cause frequent yaw motion, which results in the serious wear and tear of turret structure. As a result, regular maintenance and repair would significantly increase production costs. With a greater longitudinal scale, the relatively large bending moment of hogging and sagging will bring about the severe deformation and fatigue failure. Finally, the natural period of heave motion for the cylindrical floating body is still in the centralized area of wave energy and thus the heave motion response is very large.

Therefore recently some new concepts of ocean engineering structures are proposed. On one hand, based on the cylindrical FPSO, the auxiliary structures (such as skirts, heave plates and moon-pool, etc.) are used to improve heave motion performance. Therein the MPSO (mono-column production, storage and offloading system) is one of typical concepts [16,5–7]. On the other hand, a new concept of floating body with an innovative sandglass-type shape was presented by Huang et al. [9,10,11] Yao et al. [20] and Wang et al. [18], to solve the performance limitations of traditional ship-type and cylindrical FPSOs.

In this paper, firstly the new concept of sandglass-type FPSO is introduced. Next, by using classic boundary element method (BEM) based on potential flow theory, the effects of shape parameters on motion performance of sandglass-type model are studied. Furthermore, in order to provide guideline and scheme for the shape design of new floating body, the engineering estimation expressions of wave frequency versus minimum heave motion RAO for the new floating model are theoretically and mathematically deduced. On this basis, the basic functions of cylindrical FPSO “Sevan Piranema” (i.e., the design values of load capacity, displacement, storage space, topside area, etc.) are incorporated into the design for new sandglass-type FPSO vessels. Finally, the new sandglass-type floating body is compared with cylindrical model by numerical method and experimental analysis to verify the accuracy of the numerical method in this paper and show the advantages of hydrodynamic performance for the new sandglass-type FPSO.

2. Description of new sandglass-type FPSO

The new sandglass-type FPSO has an innovative floating body with sandglass-type shape, which has not only larger spaces of oil storage than traditional ocean platforms but also better hydrodynamic performance and adaptability to extreme sea environment than traditional ship-type and cylindrical FPSO [18]. On this basis, various modules (such as production, processing, storage, offloading, heating, living functions, etc.) are equipped on the upper deck, respectively, as shown in Fig. 1. Thus, the sandglass-type FPSO can be widely applied in various sea conditions and be better for multifunctional integration with more economic benefits.

For the new concept of sandglass-type FPSO, in order to maintain constant floating state, good stability and hydrodynamic performance for various working conditions (full load, ballast, etc.), an innovative method is presented by Huang et al. [12] to control performance of sandglass-type FPSO during offloading and loading operations, which includes a new loading and offloading technique and subdivision scheme with equal proportional volume. Then, a central cabin is settled in the middle of the main floating body, in which all kinds of pipelines can be configured for transport of oil and gas.

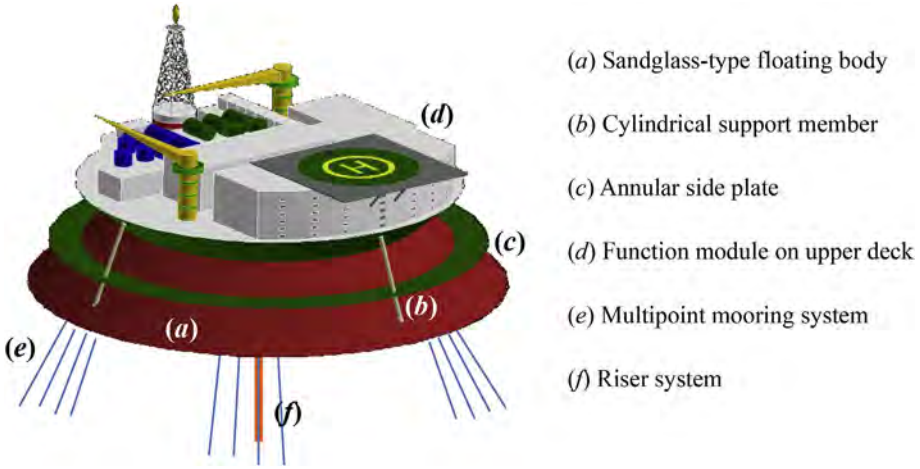

Fig. 1. Sketch of new sandglass-type FPSO.

Next, multiple water-tight tanks are uniformly distributed surrounding the center for oil storage and other functions, therein oil tanks from bottom to top are designed according to subdivision scheme with equal proportional volume. Moreover, the outer bulkhead can be designed as the double-layer form, which can not only provide extra support for the main deck but also be used as ballast-water tank to prevent the oil leakage and ensure the safety for the oil production processing. In addition, on the upper deck various functional modules (such as production, oil storage, offloading, living and power, etc.) are arranged based on the rules of classification society as shown in Fig. 2.

Furthermore, the new sandglass-type concept can make the hydrodynamic performance of FPSO to be no longer sensitive to the wave direction. Therefore a multiple-point mooring system can be taken to keep position for the lesser cost of design and maintenance. During the offloading process, on one side of the main floating body, tandem configuration as shown in Fig. 3 can be applied to connect the shuttle tanker by mooring lines and oil flexible hoses. This connection system can not only be more suitable for the severe sea conditions but also support various scales of shuttle tankers.

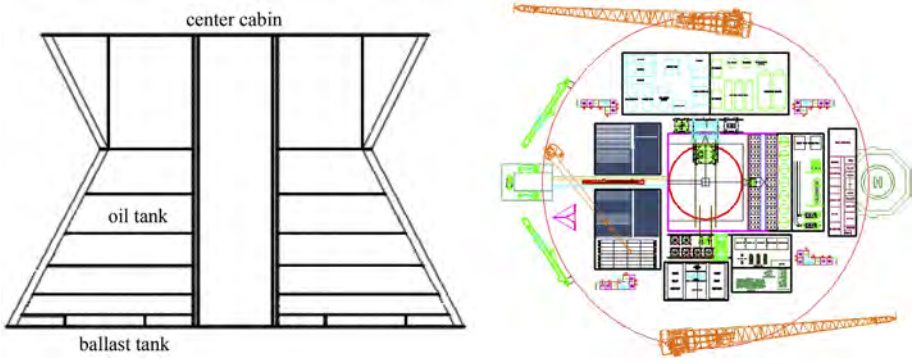

Fig. 2. Arrangement of tanks and functional modules for new sandglass-type FPSO.

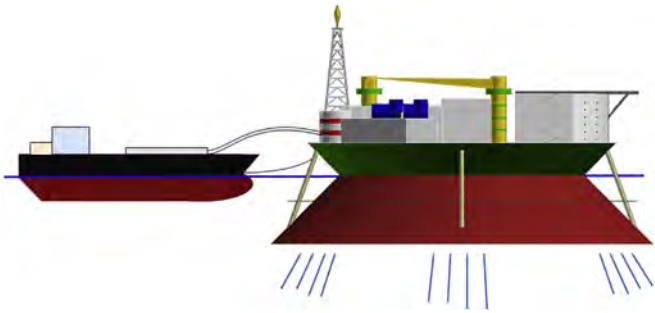

Fig. 3. Sketch of offloading and mooring system for new sandglass-type FPSO.

3. Effects of shape parameters on motion performance of sandglass-type model

Firstly, sandglass-type shape of new floating body is introduced and its numerical model is created. Then, based on wave potential theory [1,14,21], here numerical boundary element method of this paper is taken to study the effects of shape parameters on motion performance of sandglass-type model.

3.1. Sandglass-type shape and numerical model of floating body

New concept of FPSO has an innovative sandglass-type floating body, which includes nine parameters. V_T is the volume above the water plane, R_T is the radius of the top deck, f is the freeboard, β is the inclination angle of upper structure, R_w is the radius of the water plane, V_B is displacement volume, R_B is the radius of bottom, d is the draught and α is the inclination angle of substructure as shown in Fig. 4. Therein, based on geometrical relationship and five independent parameters, sandglass-type shape of floating body can be identified.

Here the accuracy of numerical method in this paper is studied with a sandglass-type floating model with V_B 350000 m^3, V_T 150000 m^3, R_T 64.5 m, α 45°, R_w 50 m. By analyzing the mesh sensitivity and considering the effect of computation precision and speed, quadrilateral meshes with 4 m size are taken on the surface of floating body as shown in Fig. 4. Furthermore, the heave and pitch motion RAOs versus two different methods are compared in Fig. 5 between numerical method of this paper and WAMIT CODE. From the figure, it can be found that the results obtained by these two methods are in good agreement with each other, which shows the accuracy and availability of numerical method in this paper.

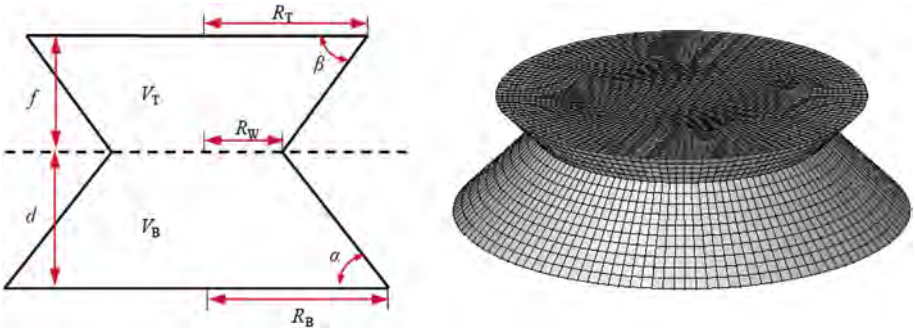

Fig. 4. Shape parameters and numerical model of sandglass-type floating body.

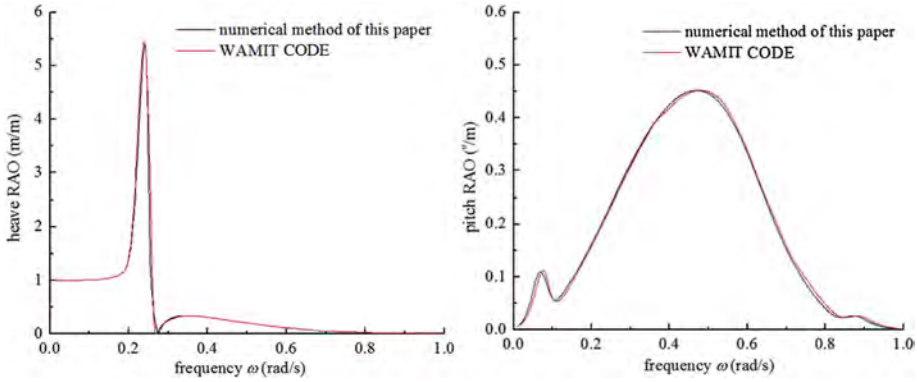

Fig. 5. Comparison of heave and pitch RAOs versus different numerical methods.

3.2. *Hydrodynamic analysis of floating models with different parameters*

Usually according to ship owner's requirement (DWT, displacement and storage space, etc.), shape parameters V_B, V_T and R_T can be selected. Furthermore, hydrodynamic performance of floating body is determined by two shape parameters α and R_w of the substructure. Thus various floating models with

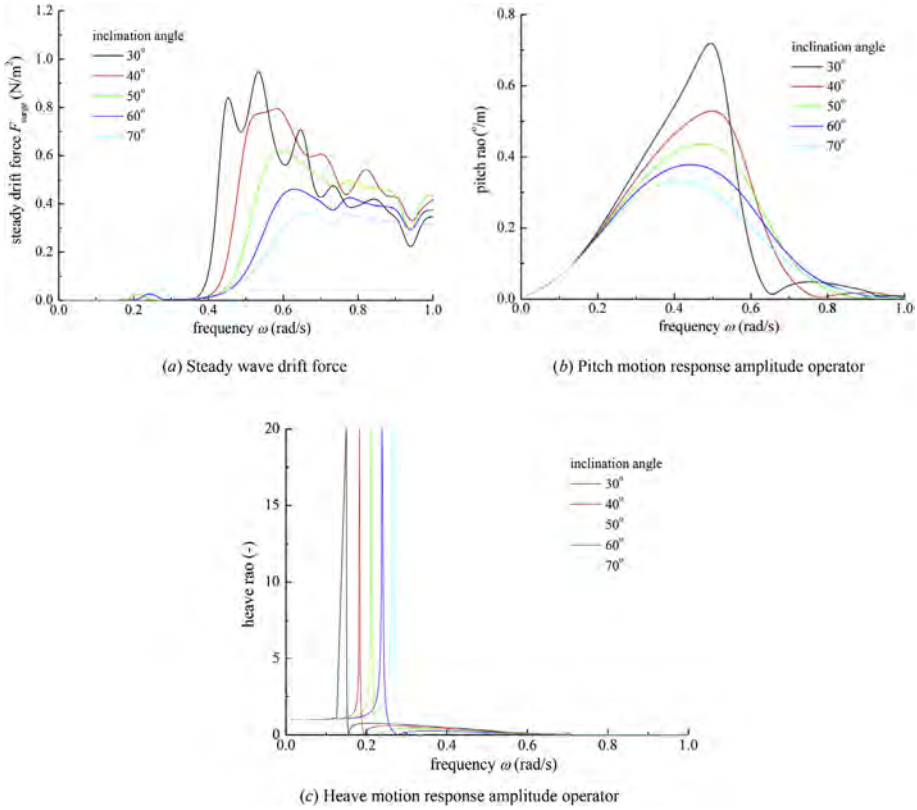

Fig. 6. Hydrodynamic performance of floating models with different inclination angles.

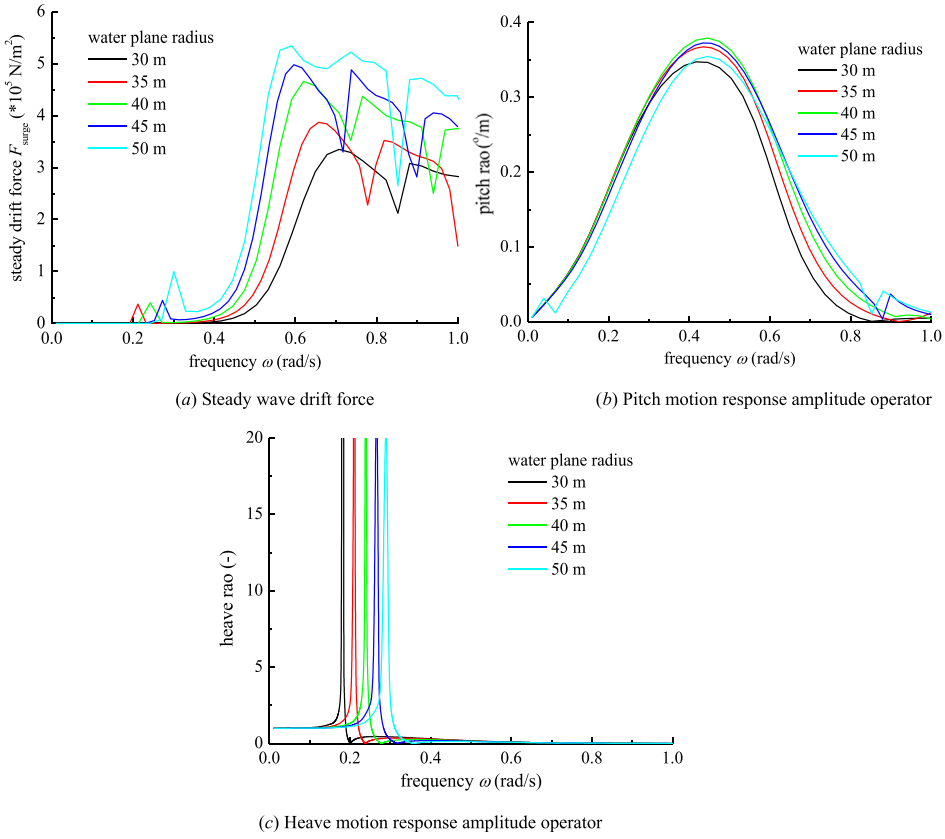

(*a*) Steady wave drift force

(*b*) Pitch motion response amplitude operator

(*c*) Heave motion response amplitude operator

Fig. 7. Hydrodynamic performance of floating models with different radii of water plane.

different α and R_w are created to study the effects of shape parameters on motion performance of sandglass-type model.

Next, V_B is taken as 350000 m^3. Hydrodynamic coefficients of different inclination angles 30° ~70° ($R_w = 40$ m) and different radii of the water plane 30–50 m ($\alpha = 60°$) are calculated. Then the steady drift forces, pitch and heave motion RAOs without viscous damping are shown in Figs. 6 and 7.

In the Fig. 6 (*a*), the steady drift force is very small in $\omega < 0.4$ rad/s and then straightly increases to the maximum value near $\omega = 0.5$–0.6 rad/s. From the Fig. 6 (*b*), pitch motion curve of response amplitude operator (RAO) presents variation trend of parabola in the frequency bandwidth $0 < \omega < 0.8$ rad/s and reaches peak near $\omega = 0.4$–0.5 rad/s. Moreover, it can be further found that the influence of shape parameters on hydrodynamic performance is obvious. The larger the inclination angle gets, the smaller the pitch motion and steady drift force in frequency bandwidth of high wave energy will be. Furthermore, from the Fig. 7 (*a*) and (*b*), reducing the radius of water plane can improve hydrodynamic performance of steady drift force and pitch motion in the centralized area of wave energy.

As shown in Fig. 6 (*c*) and 7 (*c*), the heave motion RAO of new floating model has a very narrow peak bandwidth near natural frequency and then suddenly drops on both sides. On the low-frequency zone, heave motion response stably varies about 1.0. However, on the side of the high frequency heave motion RAO tends to zero firstly, which is caused by the minimum wave excitation force. Then with the frequency gradually increasing, heave motion response rapidly changes and has second highest peak which should be much smaller than the maximum value. Moreover, it can be further found that by

decreasing the inclination angle α or radius of the water plane R_w, the natural frequency of heave motion is smaller and more likely to be far away from frequency bandwidth of wave energy. However, to further reduce the inclination angle or radius of the water plane can increase the second highest peak of heave motion RAO, which shows that the relative position between the frequency of heave maximum and minimum and wave energy concentration zone could determine the heave motion performance of new FPSO. Therefore, it is very important and necessary to perform more detailed analysis about heave motion performance of new sandglass-type floating body.

4. Further discussion on heave motion performance of sandglass-type floating body

Here, in order to search a convenient and available design scheme for model shape to control and improve the heave motion performance of sandglass-type floating body, further discussion on hydrodynamic parameters of heave motion is made.

Due to the difficulty of calculation accurately on viscous damping and coupled heave-pitch nonlinear stiffness, firstly the wave frequency versus minimum heave motion RAO, which not only decides the position of maximum peak and second highest peak but also can be less affected by viscous damping and nonlinear stiffness, is selected as the key parameter to control heave motion. Secondly based on the airy wave theory [3,15] and the research of [13]; the convenient and available estimation expressions of the frequency versus minimum heave motion RAO are deduced. Finally, on this basis the design guideline and scheme of sandglass-type shape are analyzed and proposed.

4.1. Influence of viscous damping and nonlinear stiffness on heave motion RAO

By introducing the estimated viscous damping and simplified nonlinear stiffness, the heave motion equation of sandglass-type floating model can be described as follows,

$$(M + A_{33})\ddot{X}_3 + B_{33}\dot{X}_3 + B_h\dot{X}_3\left|\dot{X}_3\right| + K'_{33}X_3 = F_3 \tag{1}$$

therein A_{33} is heave added mass, B_{33} heave radiation damping and F_3 is heave wave exciting force, which are obtained by numerical boundary element method based on wave potential theory of this paper. B_h as viscous damping of heave motion can be simply achieved by

$$B_h = B_d^h \rho \pi D^2/8 \tag{2}$$

Where B_d^h is vertical drag coefficient which is selected as 0.57 by referring to the research of Ref. [23] about Spar platform. D is the radius of bottom, ρ is the fluid density.

Furthermore, the nonlinear hydrostatic stiffness K'_{33} can be calculated by equation (3) and the information of transient waterline is shown in Fig. 8.

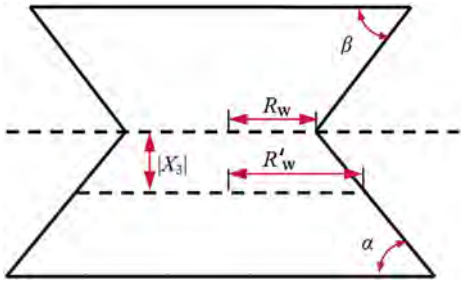

Fig. 8. Information of water plane for floating body with sandglass-type shape.

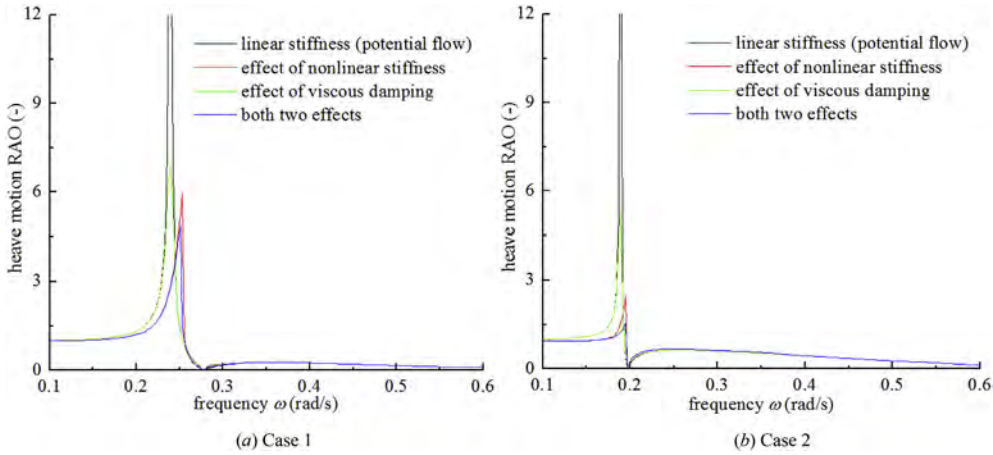

Fig. 9. Comparison of heave motion RAOs versus different floating models.

$$K'_{33} = \begin{cases} \rho g \pi (R_W + X_3 \mathrm{ctg}\beta)^2 & X_3 \geq 0 \\ \rho g \pi (R_W - X_3 \mathrm{ctg}\alpha)^2 & X_3 < 0 \end{cases} \tag{3}$$

Here take two floating models for test cases. Case 1 is V_B 350000 m^3, V_T 150000 m^3, R_T 51.8 m, α 60° and R_w 40 m. Case 2 is V_B 350000 m^3, V_T 150000 m^3, R_T 70.5 m, α 30° and R_w 50 m. By numerical Runge-Kutta method, the different heave motion RAOs are studied and described in Fig. 9. From the figure, it can be found that viscous damping and nonlinear stiffness have relative large effect on the value and corresponding frequency of maximum RAO. But the corresponding frequencies ($\omega_{\min}$) of the minimum RAO versus different stiffness and damping are almost the same and thus can be used and chosen as the key parameter to control the heave motion performance.

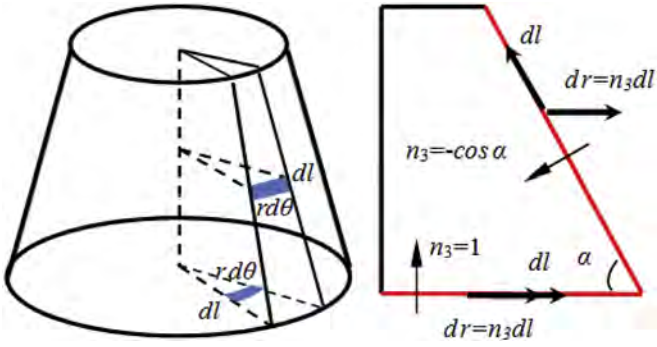

Fig. 10. Sketch of surface and line integral on the submerged floating body.

4.2. Deduction for estimation expression of frequency versus minimum heave motion RAO

By means of airy wave theory, the heave incident wave force, heave diffraction wave force, added mass and the corresponding frequencies ($\omega_{\min}$) of the minimum RAO are studied respectively.

4.2.1. Heave incident wave force

Assume that the complex function of incident potential can be written as follow,

$$\varphi_I = \frac{ig\xi}{\omega} e^{ikx} e^{kz} e^{i\omega t} \tag{4}$$

Where, ξ is wave amplitude, ω is wave frequency and k is wave number. Then the incident wave force on new floating body can be expressed,

$$\begin{aligned} F_I &= -\rho \iint_S n_3 \frac{\partial \varphi_I}{\partial t} ds = -\rho \iint_S n_3 \frac{ig\xi}{\omega} e^{ikx} e^{kz} e^{i\omega t} (i\omega) ds \\ &= \rho g \xi e^{i\omega t} \iint_S n_3 e^{ikx} e^{kz} ds \end{aligned} \tag{5}$$

As shown in Fig. 10, the area of surface element on the body surface of new floating model is $r\,d\,\theta\,dl$, and then the equation (5) can be converted into double integral along red (in web version) line and angle respectively. Then based on the geometrical relationship of line integral $d\,r = n_3\,dl$ can be achieved and thus the equation (5) can be represented as,

$$\begin{aligned} F_I &= \rho g \xi e^{i\omega t} \int_\theta \int_l n_3 e^{ikr\cos\theta} e^{kz} r d\theta dl \\ &= \rho g \xi e^{i\omega t} \int_\theta \int_r e^{ikr\cos\theta} e^{kz} r d\theta dr \\ &= \rho g \xi e^{i\omega t} \int_r \left(\int_\theta e^{ikr\cos\theta} d\theta \right) e^{kz} r dr \end{aligned} \tag{6}$$

Then the $e^{ikr\cos\theta} = \cos(kr\cos\theta) + i\sin(kr\cos\theta)$ in equation (6) should be further derived by using the series,

$$\cos(kr\cos\theta) = 1 - \frac{(kr\cos\theta)^2}{2!} + \frac{(kr\cos\theta)^4}{4!} - \cdots + (-1)^n \frac{(kr\cos\theta)^{2n}}{(2n)!} + \cdots \tag{7}$$

$$\sin(kr\cos\theta) = kr\cos\theta - \frac{(kr\cos\theta)^3}{3!} + \frac{(kr\cos\theta)^5}{5!} - \cdots + (-1)^{m-1} \frac{(kr\cos\theta)^{2m-1}}{(2m-1)!} + \cdots \tag{8}$$

In the frequency band of $\omega \le 0.35$ rad/s, the 4th and higher order term in equation (7) can be neglected and $\int_0^{2\pi} \sin(kr\cos\theta) d\theta = 0$ can be obtained, which are introduced into equation (6).

$$F_I = \rho g \xi e^{i\omega t} \int_r \left(\int_\theta \left\{ \left[1 - \frac{(kr\cos\theta)^2}{2} + \ldots \right] + i \left[kr\cos\theta - \frac{(kr\cos\theta)^3}{6} + \ldots \right] \right\} d\theta \right) e^{kz} r dr$$
$$\approx \rho g \xi e^{i\omega t} \int_r \left[2\pi \left(1 - \frac{(kr)^2}{4} \right) \right] e^{kz} r dr = 2\pi \rho g \xi e^{i\omega t} \int_r \left[1 - \frac{(kr)^2}{4} \right] e^{kz} r dr \tag{9}$$

Furthermore based on the research of Korvin-Kroukovshy and Jacobs, the 1-$(k\,r)^2/4$ can be removed from integral sign and then the approximate estimation formula (10) of heave incident wave force for new sandglass-type floating body can be deduced.

$$F_I \approx 2\pi \rho g \xi e^{i\omega t} \left[1 - \frac{(kr_0)^2}{4} \right] e^{-kd(1+\delta)} \int_r r dr$$
$$= \rho g \pi R_W^2 \xi e^{i\omega t} \left[1 - \frac{(kr_0)^2}{4} \right] e^{-kd(1+\delta)} \tag{10}$$

where δ=(R_B-R_W)/R_W, r_0=(R_B+R_W)/2, d is draft of floating body. Therein, R_W is the water-plane radius, and R_B is the radius of bottom surface.

4.2.2. Heave diffraction wave force

Here based on wave diffraction and radiation theory second Green formula, the heave diffraction wave force of sandglass-type floating body can be written as,

$$F_D = -\rho \iint_S n_3 \frac{\partial \varphi_D}{\partial t} ds = -\rho \iint_S n_3 i\omega \varphi_D ds \tag{11}$$

In this equation, the boundary condition on body surface $\partial\varphi_3/\partial n = i\omega n_3$ of radiation potential φ_3 is introduced and equation can be recast as,

$$F_D = -\rho \iint_S \frac{\partial \varphi_3}{\partial n} \varphi_D ds \tag{12}$$

According to the second Green formula $\iint \varphi \frac{\partial \varphi}{\partial t} ds = \iint \varphi \frac{\partial \varphi}{\partial t} ds$ and wall boundary condition of diffraction potential $\frac{\partial \varphi_I}{\partial n} = -\frac{\partial \varphi_D}{\partial n}$, the equation (12) can be further rewritten as follows.

$$F_D = -\rho \iint_S \frac{\partial \varphi_D}{\partial n} \varphi_3 ds = \rho \iint_S \frac{\partial \varphi_I}{\partial n} \varphi_3 ds \tag{13}$$

Furthermore, by the equation (4) of incident potential and its directional derivative $\frac{\partial \varphi_I}{\partial n} = n_3 k \varphi_I$, the equation can be written.

$$F_D = \rho \iint_S n_3 k \varphi_I \varphi_3 ds = \rho \iint_S n_3 k \varphi_3 \frac{ig\xi}{\omega} e^{kz} e^{ikx} e^{i\omega t} ds$$
$$= \rho \omega \xi i e^{i\omega t} \iint_S n_3 \varphi_3 e^{kz} e^{ikx} ds \tag{14}$$

As shown in Fig. 9, the surface integral of equation (14) can be converted into double integral of line and angle.

$$F_D = \rho\omega\xi i e^{i\omega t}\int_\theta\int_l n_3 e^{ikr\cos\theta}e^{kz}\varphi_3 r d\theta dl = \rho\omega\xi i e^{i\omega t}\int_l\left(\int_\theta e^{ikr\cos\theta}d\theta\right)n_3 e^{kz}\varphi_3 r dl \tag{15}$$

Here the series expansion (7) and (8) of $\int_\theta e^{ikr\cos\theta}d\theta$ can be adopted and equation (15) can be rewritten as,

$$F_D \approx 2\pi\rho\omega\xi i e^{i\omega t}\int_l\left[1-\frac{(kr)^2}{4}\right]n_3 e^{kz}\varphi_3 r dl \tag{16}$$

For the engineering application, the conclusions of Korvin-Kroukovshy and Jacobs can be referred and the approximate expression of heave diffraction wave force can be achieved.

$$F_D \approx 2\pi\rho\omega\xi i e^{i\omega t}\left[1-\frac{(kr_0)^2}{4}\right]e^{-kd}\int_l n_3\varphi_3 r dl \tag{17}$$

where $r_0=(R_B+R_W)/2$, d is draft, R_W is radius of water plane and R_B is radius of bottom surface.

Furthermore, the heave radiation wave force T_{33} can be obtained by the potential flow theory.

$$T_{33} = \omega^2 A_{33} - i\omega B_{33} = -\rho\iint_S n_3 i\omega\varphi_3 ds = -\rho\int_\theta\int_l n_3 i\omega\varphi_3 r dl d\theta = -2\pi\omega i\omega\int_l n_3\varphi_3 r dl \tag{18}$$

where A_{33} is heave added mass, B_{33} is heave radiation damping. Thus the integral of equation (14) is obtained.

$$\int_l n_3\varphi_3 r dl = -\frac{\omega^2 A_{33} - i\omega B_{33}}{2\pi\rho i\omega} \tag{19}$$

Take the equation (19) into the (17), and then the diffraction wave force can be obtained.

$$F_D = -\xi e^{i\omega t}\left[1-\frac{(kr_0)^2}{4}\right]e^{-kd}\left(\omega^2 A_{33} - i\omega B_{33}\right) \tag{20}$$

Moreover, in the case of the new sandglass-type floating body, the added mass is estimated by using the method given by Hooft (1982) [8]. Furthermore, the shape parameter of inclination angle is introduced to obtain the engineering estimation formula for heave added mass,

$$A_{33} = \frac{1}{3}\pi\rho R_B^3 + \left(\frac{1}{3}\pi\rho R_B^3 - \frac{1}{3}\pi\rho R_W^3\right)\ max(ctg\alpha,\ 1) \tag{21}$$

where α is the inclination angle of submerged floating body.

4.2.3. Frequency versus minimum heave motion RAO

Because the frequency versus minimum heave RAO is less affected by viscous damping and nonlinear stiffness, the heave motion response of sandglass-type floating body under the linear regular wave can be calculated by neglecting viscous effect and nonlinear stiffness,

$$(M + A_{33})\ddot{x}_3 + B_{33}\dot{x}_3 + K_{33}x_3 = F_3 \tag{22}$$

where $\ddot{x}_3$, $\dot{x}_3$ and x_3 are the acceleration, velocity and displacement of heave motion, respectively; A_{33}, B_{33} and K_{33} are added mass, radiation damping and hydrostatic restoring stiffness of heave motion, and F_3 is the heave excitation wave force on floating body.

Furthermore, by introducing equations (10) and (20), the heave motion RAO can be described as follows,

$$\begin{aligned}\frac{x_3}{\xi} &= \frac{|F_3|}{\xi\sqrt{\left(K_{33} - (M + A_{33})\omega^2\right)^2 + (B_{33}\omega)^2}} \\ &= \frac{\left[1 - \frac{(kr_0)^2}{4}\right]e^{-kd}\sqrt{\left(\rho g A_W - \rho\omega^2 A_W z_0 - \omega^2 A_{33}\right)^2 + (\omega B_{33})^2}}{\sqrt{\left(K_{33} - (M + A_{33})\omega^2\right)^2 + (B_{33}\omega)^2}}\end{aligned} \tag{23}$$

where Aw is area of water plane, $z_0 = \delta d$, $\delta = (R_B\text{-}R_W)/R_W$, R_W is the radius of the water plane, R_B is the radius of bottom, d is the draught.

By analyzing the (23) of heave motion, the frequency ω_{min} corresponding to minimum RAO can be obtained.

$$\begin{aligned}\omega_{\min}^2 &= \frac{2\rho g A_W(\rho A_W z_0 + A_{33}) - B_{33}^2}{2(\rho A_W z_0 + A_{33})^2} \\ &= \frac{\rho g A_W}{(\rho A_W z_0 + A_{33})}\left[1 - \frac{B_{33}^2}{2(\rho A_W z_0 + A_{33})\rho g A_W}\right]\end{aligned} \tag{24}$$

Furthermore, because the heave radiation damping B_{33} near the frequency ω_{min} is approximately zero. Thus in the equation (24) the B_{33} can be neglected and the frequency ω_{min} can be achieved,

$$\omega_{\min} \approx \sqrt{\frac{\rho g A_W}{(\rho A_W z_0 + A_{33})}} \tag{25}$$

4.3. Design guideline and scheme of floating body

The heave motion performance of new floating body is also associated with practical sea condition, so here the characteristic of wave spectrum should be studied by taking the dual-parameter Pierson–Moskowitz (P–M) spectrum for example.

$$S(\omega) = \frac{1}{2\pi}\frac{H_S^2}{4\pi T_Z^4}\left(\frac{2\pi}{\omega}\right)^5 \exp\left(-\frac{1}{\pi T_Z^4}\left(\frac{2\pi}{\omega}\right)^4\right) \tag{26}$$

where ω is wave frequency, H_S is significant wave height, T_Z is average period, $S(\omega)$ is density of wave spectrum.

Then, the frequency bandwidth of concentrated wave energy (ω_L~ ω_H) is studied. Therein, the initial frequency ω_L can be described as,

$$\omega_L = \left(-\frac{1}{\pi T_Z^4} \frac{(2\pi)^4}{\ln \mu} \right)^{\frac{1}{4}} \tag{27}$$

where the variable of energy percentage μ can be defined by equation (28) and here selected as 1%.

$$\mu = \frac{\int_0^{\omega_L} \frac{1}{2\pi} \frac{H_S^2}{4\pi T_Z^4} \left(\frac{2\pi}{\omega}\right)^5 \exp\left(-\frac{1}{\pi T_Z^4} \left(\frac{2\pi}{\omega}\right)^4 \right) d\omega}{\int_0^{\infty} \frac{1}{2\pi} \frac{H_S^2}{4\pi T_Z^4} \left(\frac{2\pi}{\omega}\right)^5 \exp\left(-\frac{1}{\pi T_Z^4} \left(\frac{2\pi}{\omega}\right)^4 \right) d\omega} \tag{28}$$

Based on the conclusions of heave motion performance for new sandglass-type floating body in Section 3.2–4.2, it can be achieved that the frequency ω_{min} for the minimum heave motion RAO should be slightly less than or equal to the initial frequency ω_L of wave spectrum, in order to not only control the maximum RAO peak (natural frequency) to stay away from the bandwidth of high wave energy but also guarantee to reduce the second highest peak of heave motion RAO as possible.

$$\omega_{\min} \approx \sqrt{\frac{\rho g A_W}{(\rho A_W z_0 + A_{33})}} \approx \omega_L = \left(-\frac{1}{\pi T_Z^4} \frac{(2\pi)^4}{\ln \mu} \right)^{\frac{1}{4}} \tag{29}$$

Furthermore, due to the above-mentioned analysis on the heave motion, pitch motion and steady drift force, by introducing the intact stability criteria of ship classification society for ocean engineering structure, the design guideline for new sandglass-type floating body can be made as follows.

1. Follow the equation (29) to improve the heave motion performance;
2. Satisfy the intact stability criteria of ship classification society and retain margin to maintain enough stability;
3. Based on the guideline 1 and 2, design the inclination angle as large as possible to decrease the heave motion response, pitch motion response and steady drift force in frequency bandwidth of high wave energy.
4. Based on the guideline 1 and 2, design the radius of the water plane as small as possible to decrease the heave motion response, pitch motion response and steady drift force in frequency bandwidth of high wave energy.

On this basis, by taking the inclination angle and the radius of the water plane of floating body as loop variables, the design scheme of sandglass-type floating body is made and shown as Fig. 11.

5. Validation of test cases and discussion

In order to better verify the validaty of design guideline and scheme of new sandglass-type floating body, two test cases are designed and calculated by numerical method and engineering estimation formula. Furthermore, by taking cylindrical floating model of “Sevan Piranema” FPSO for test case, the new sandglass-type floating model with the same basic functions (displacement, storage space, upper deck area, etc.) is designed by the guideline and scheme in this paper. Finally, the hydrodynamic performance and stability of the two floating models are studied and compared by numerical and experimental method.

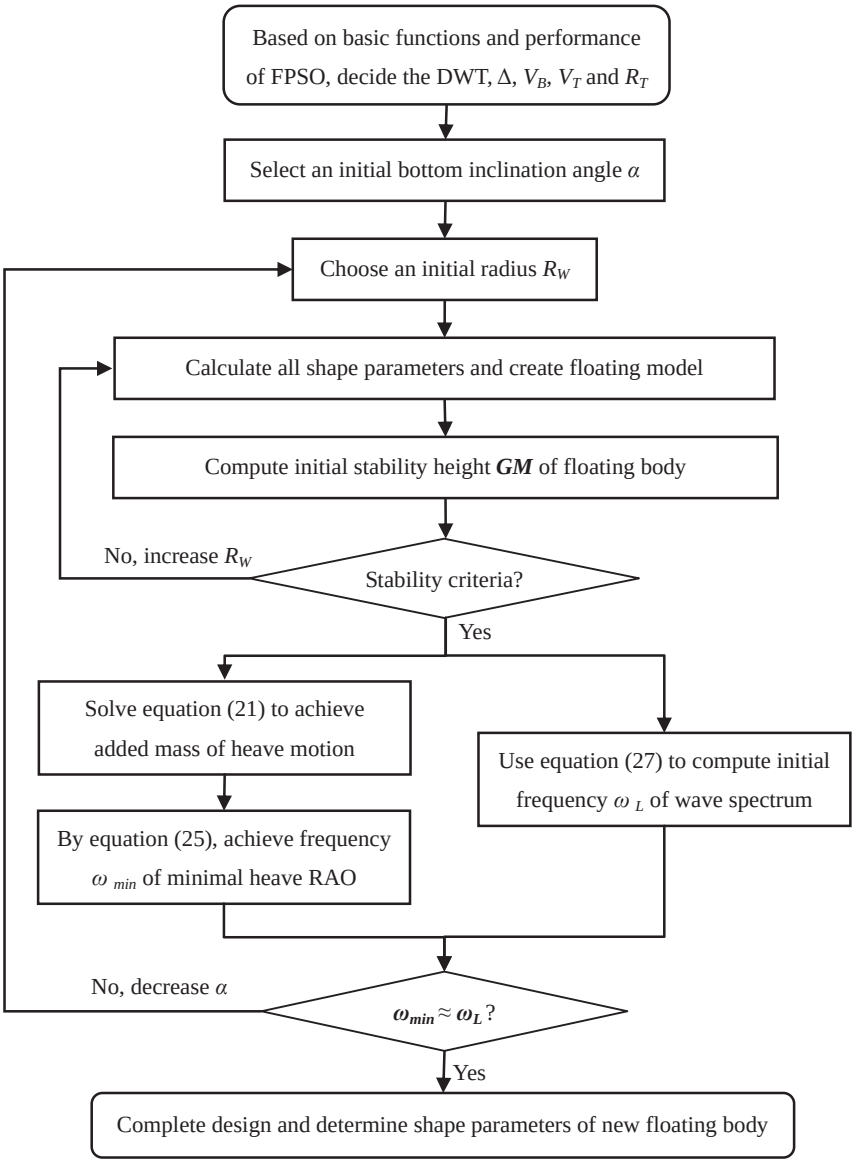

Fig. 11. Design scheme for shape parameters of new sandglass-type floating body.

Table 1
Shape parameters of sandglass-type floating model.

	Displacement volume V_B (m^3)	Radius of water plane R_W (m)	Bottom inclination angle α (°)
Model 1	367,151.22	50	30
Model 2	367,151.22	50	40

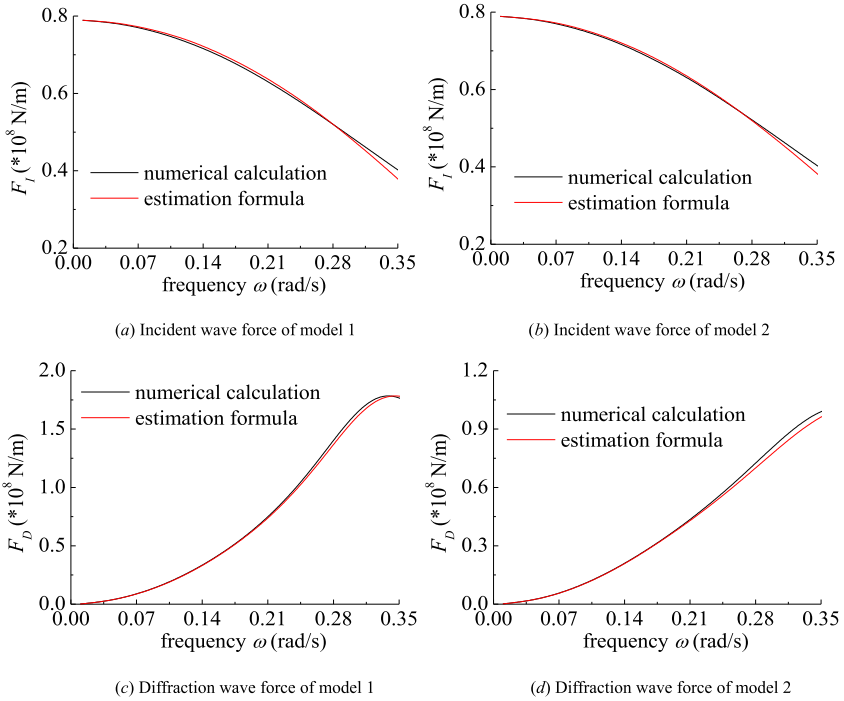

(*a*) Incident wave force of model 1

(*b*) Incident wave force of model 2

(*c*) Diffraction wave force of model 1

(*d*) Diffraction wave force of model 2

Fig. 12. Comparison of wave incident and diffraction forces versus different methods.

5.1. *Verification for design guideline and scheme of sandglass-type floating body*

In this paper, two sandglass-type floating models with different shape parameters are designed as test cases (see Table 1) to analyze the accuracy of estimation equations (10), (20), (21) and (25). Then the wave incident and diffraction forces in frequency band $\omega \leq 0.35$ rad/s versus two different methods of numerical boundary element method and estimation equations of this paper are calculated and compared in Fig. 12. In this figure, the difference of wave incident and diffraction forces by two methods is very small, which shows that on computational precision the results are almost the same. Thus, the estimation equations (10) and (20) for wave exciting force are enough accuracy to satisfy the precision requirement in engineering.

Furthermore, the heave added mass A_{33} and corresponding frequency $\omega_{\min}$ for minimum RAO by estimation equations and the numerical boundary element method are listed in Table 2. From the table, it can be found that the relative errors from the two models are below 5%. Therefore, if engineering estimation equations (21) and (25) are applied to calculate A_{33} and $\omega_{\min}$, the solutions can meet the accuracy requirement in engineering.

Table 2
Comparison of A_{33} and $\omega_{\min}$ versus different methods.

	A_{33} (10^8 kg)		Relative error	ω_{min} (rad/s)		Relative error
	BEM	Estimation formula		BEM	Estimation formula	
Model 1	18.70	19.10	2.63%	0.196	0.198	1.23%
Model 2	11.70	10.50	4.64%	0.249	0.251	0.88%

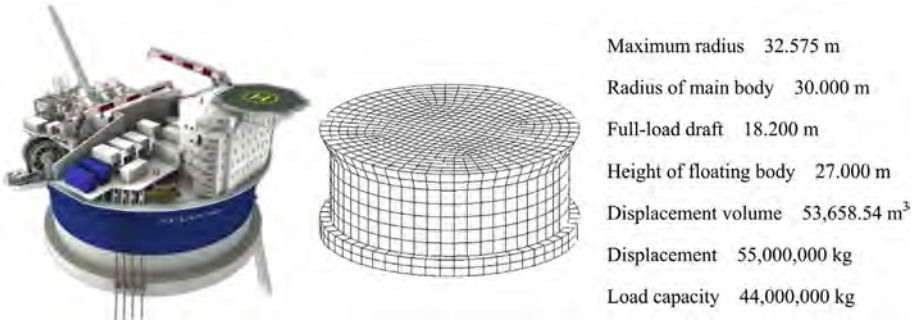

Fig. 13. Hydrodynamic model and main dimensions of cylindrical FPSO.

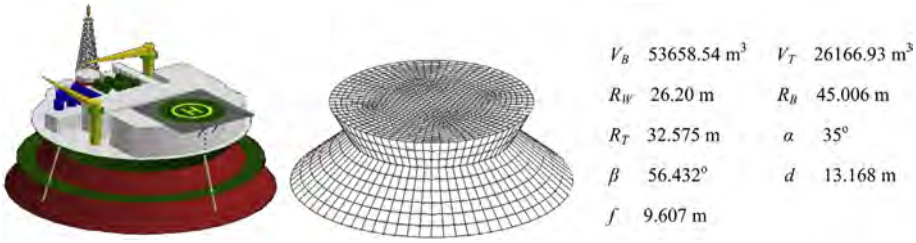

Fig. 14. Hydrodynamic model and shape parameters of new sandglass-type floating model.

5.2. Comparison of cylindrical and new sandglass-type floating models

In order to discuss the hydrodynamic performance and stability of new sandglass-type FPSO, here based on the functions of "Sevan Piranema" FPSO and hydrodynamic model as shown in Fig. 13, a new sandglass-type floating model (see Fig. 14) with the same load capacity, displacement, storage space, and topside area is obtained by the design scheme of this paper.

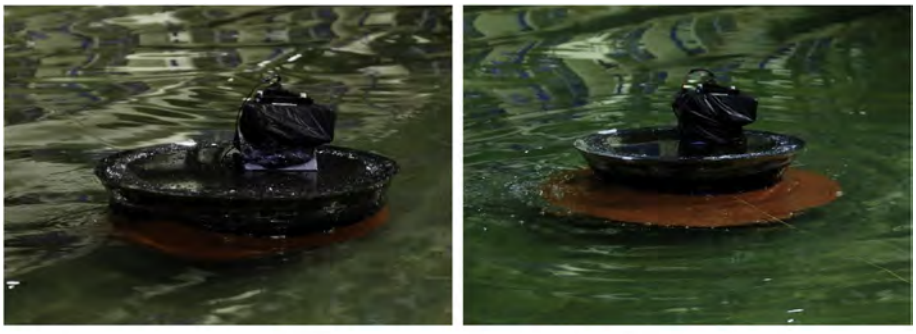

(*a*) cylindrical floating model (*b*) new sandglass-type floating model

Fig. 15. Experimental model of cylindrical and sandglass-type floating body.

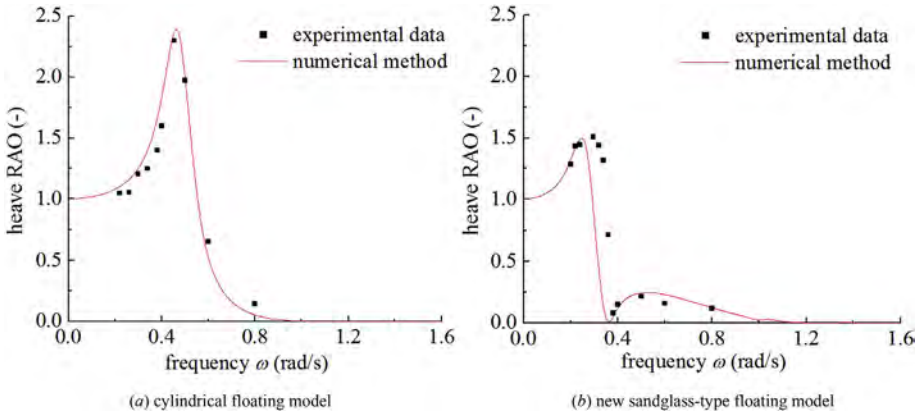

Fig. 16. Comparison of heave motion RAO versus different floating models and methods.

5.2.1. Motion performance RAOs of two floating models

Here the hydrodynamic performances of two floating models are studied by two methods of the numerical boundary element and experimental methods. Therein, the experiment (1:70 scale model) has been done in the state key laboratory of coastal and offshore engineering of Dalian University of Technology as shown in Fig. 15.

With the numerical boundary element and experimental data, the heave motion RAO of cylindrical and sandglass-type floating models are calculated and shown in Fig. 16. From the figure, it can be found that the difference of results by two methods is very small, which shows that the numerical method is accurate enough to study the heave performance of floating model. Furthermore, it can be also seen that the maximum peak of heave motion RAO for cylindrical model is totally located in the frequency band (0.35 rad/s $<\omega < 0.8$ rad/s) of high wave energy in the South China Sea, which should result in the large heave motion response of cylindrical model. On the other hand, the heave motion RAO of new sandglass-type floating body has a narrow maximum bandwidth near $\omega = 0.25$ rad/s and then sharply reduces on the both sides. Therein, in the high-frequency side, with the frequency gradually being high, the heave motion RAO rapidly increases from minimum to the second highest peak, which is about 0.2 and much less than the maximum 1.5. Thus for the new sandglass-type floating model, the maximum of heave motion RAO can be away from the concentration zone of wave spectrum, which can substantially improve the heave motion performance of FPSO.

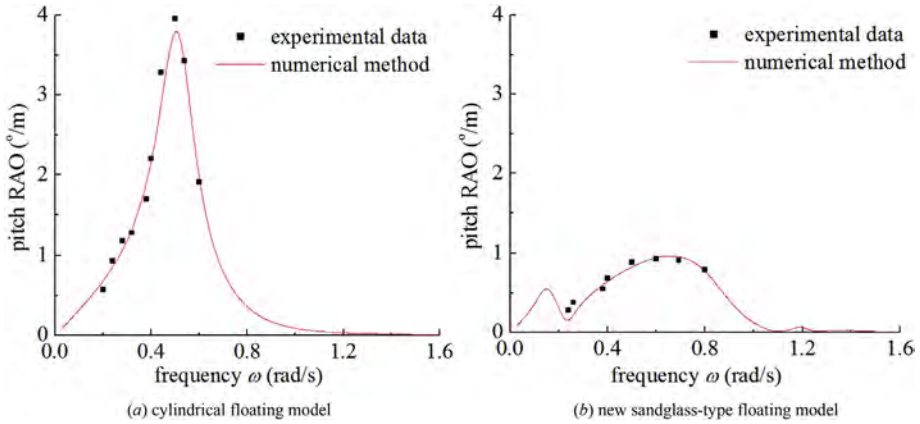

Fig. 17. Comparison of pitch motion RAO versus different floating models and methods.

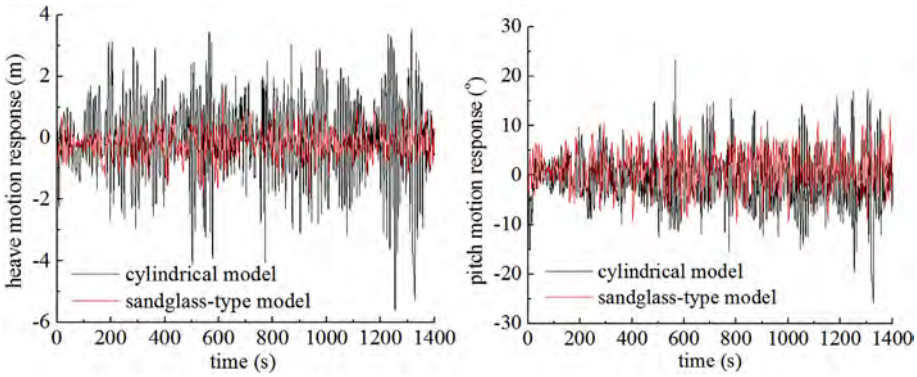

Fig. 18. Time history of heave and pitch motion responses for two floating models in experiments.

Furthermore, the Fig. 17 shows the comparison of pitch motion RAO versus cylindrical and new sandglass-type floating models by experimental and numerical methods. From the figure it can be found that the pitch RAOs versus two different methods are in good agreement with each other, which shows that the numerical method is accurate enough to study the pitch motion performance of floating model. Moreover, it also can be seen that the maximum peak (natural frequency) of pitch motion RAO for the cylindrical floating model is near $\omega = 0.5$ rad/s, which lies in the high energy band (0.35 rad/s $<\omega <$ 0.8 rad/s) of the wave spectrum. Thereby, the cylindrical floating model may generate a relative large pitch motion response, which should need very high and serious requirements for the center-of-gravity control in the design process. However, the contour design of the sandglass-type floating body can greatly improve the added mass and damping of pitch motion, which can effectively reduce the maximum peak of pitch motion RAO and thus enhance the pitch motion performance of FPSO. Especially, the natural frequency of pitch motion for the new model is about 0.1 rad/s and can avoid the frequency bandwidth of high wave energy. But it should be noted that the effect of wave drift force on the pitch motion should be important and needed to be mainly considered in future.

5.2.2. Motion response of two floating models in the sea condition of once in a year

Here, firstly time histories of heave and pitch motion responses in experiments for cylindrical and sandglass-type floating models under the sea condition of once in a year in the South China Sea

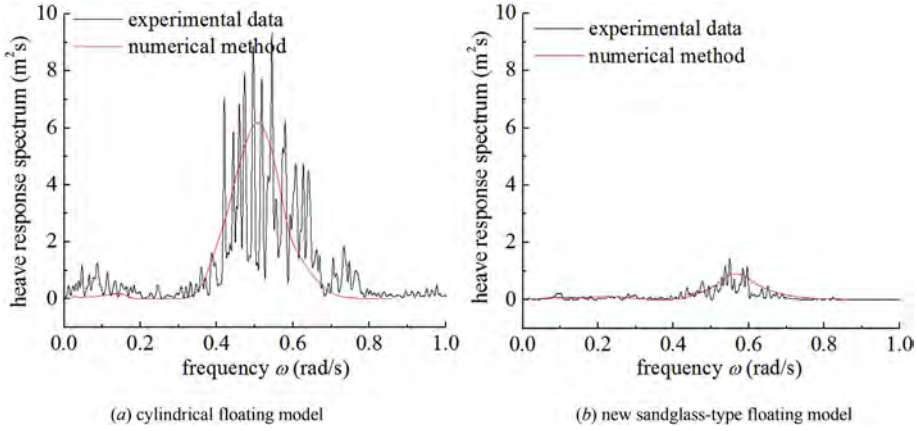

Fig. 19. Motion spectrum of heave motion versus different models and methods.

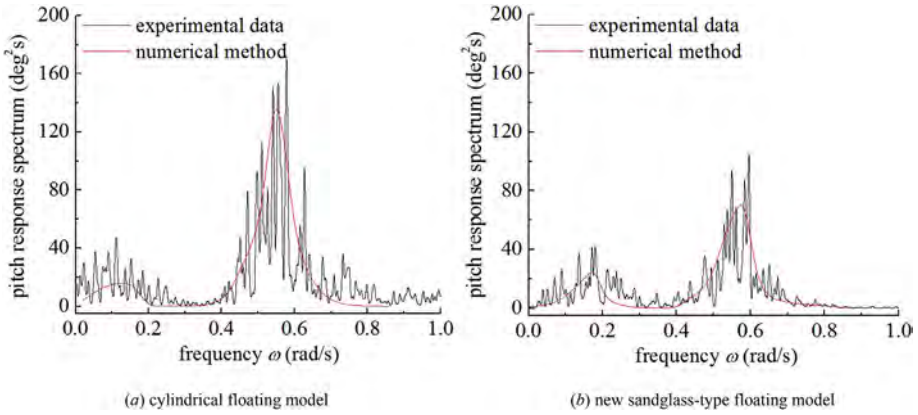

Fig. 20. Motion spectrum of pitch motion versus different models and methods.

($Hs = 6.2$ m, $T\,p = 11.1$ s in Ref. [18] are shown in Fig. 18. Then based on the experimental data and Fast Fourier Transform (FFT) method, the heave and pitch motion spectrums can be achieved and described in Figs. 19 and 20 along with the numerical solutions of this paper by frequency-spectrum analysis method. Furthermore, the standard deviations of heave and pitch motion for the two models and two methods are analyzed and listed in Table 3.

From the Figs. 19 and 20 and Table 3, it can be found that the differences of motion performance for the two floating models between numerical and experimental methods are less than 10%, which satisfies the engineering precision requirement and validates the accuracy of numerical method. Furthermore, the new sandglass-type model can reduce to about 1/3 the heave motion response of cylindrical model and the pitch motion response decreases by about 50%, which shows that the shape design of sandglass-type floating body can effectively and significantly enhance the operation performance of FPSO under the working condition.

5.2.3. Stability of two floating models

Here by classic variable displacement method of [22]; stability curves of cylindrical and sandglass-type floating models are calculated and drawn in Fig. 21. Then based on the stability curves, the characteristic parameters of the two models can be analyzed and shown in Table 4.

In the table, compared with cylindrical model, the new floating model can not only satisfy the IMO Stability criteria about initial stability but also provide smaller natural frequency and more moderate pitch motion. Then with the heeling angle gradually increasing, the restoring moment of sandglass-type model rapidly enlarges. Furthermore, compared with cylindrical model, the maximum restoring moment of new model can be enhanced by over 50% and the limiting wind moment can

Table 3
Standard deviations of heave and pitch motion for two models and two methods.

Heave motion response (m)	Sandglass-type model	Cylindrical model	Ratio
Experiment analysis	0.46	1.24	1:2.70
Numerical simulation	0.44	1.29	1:2.93
Relative error	−4.35%	4.03%	
Pitch motion response (°)	**Sandglass-type model**	**Cylindrical model**	**Ratio**
Experiment analysis	3.68	5.38	1:1.46
Numerical simulation	3.36	5.25	1:1.56
Relative error	−8.70%	−2.42%	

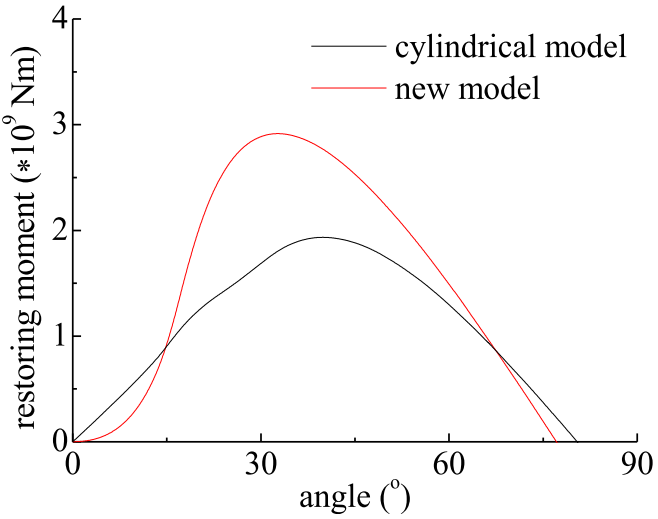

Fig. 21. Comparison of stability curves versus two different models.

Table 4
Characteristic parameters of stability curves versus two different models.

	Sandglass-type model	Cylindrical model
Initial stability height (m)	0.360	5.894
Maximum restoring moment ($\times 10^9$ Nm)	2.920	1.940
Limiting heeling angle (°)	32.000	40.000
Vanishing angle of stability (°)	77.000	80.000
Curve area ($\times 10^{11}$ m^2)	1.220	0.929
Limiting wind moment ($\times 10^9$ Nm)	1.295	0.928

increase by about 40%. Thus the new sandglass-type floating body has better stability characteristic for severe deep-water environment.

6. Conclusion

In order to solve the performance limitations of traditional ship-type and cylindrical FPSO, this paper presents a new concept FPSO with innovative sandglass-type floating body. Then the hydrodynamic performances of new floating model are studied by the qualitative and quantificational analysis. Furthermore, based on the design scheme and functions of cylindrical FPSO "Sevan Piranema", a new sandglass-type floating body can be achieved and discussed by numerical and experimental methods. Finally, many useful conclusions can be made as follows.

1. The engineering estimation expressions of heave wave excitation force and frequency corresponding to the minimum heave motion RAO are derived by potential flow theory. Furthermore, the relative error between estimation results and numerical solutions is less than 10%, which shows that the engineering estimation expression can meet the precision requirement of practical engineering and it will be further chosen as a design guideline to control the heave motion performance of sandglass-type floating body.
2. Based on the guideline and scheme, a new sandglass-type floating body is designed and compared with "Sevan Piranema" cylindrical model by numerical and experimental methods.

1) The design of sandglass-type floating body can make the maximum peak of heave motion RAO away from the frequency bandwidth of wave spectrum with high energy, and thus can significantly improve the heave motion performance. For the full-load FPSO under sea condition of once in a year, the new model can reduce to about 1/3the heave motion response of cylindrical model. Furthermore because the FPSO with drilling function is much concerned about the heave motion response, therefore the shape design of sandglass-type model in this paper can provide a potential effective solution to improve the heave motion performance of FDPSO.
2) The design of sandglass-type floating body can greatly increase added mass and radiation damping of pitch (roll) motion, which can effectively restrain the occurrence of maximum peak in the high wave frequency and thus improve the pitch motion performance. For the full-load FPSO under sea condition of once in a year, the new sandglass-type model can decrease by about 50% the pitch motion response of cylindrical model. Therefore the new floating model can not only efficiently improve both the working performance and the safety of FPSO but also reduce the difficulty of COG control in the general arrangement.
3) The design of sandglass-type floating body can not only achieve smaller natural frequency of pitch motion but also provide the larger maximum restoring moment and endure the larger limiting wind moment. Thus the new floating model can support better stability characteristic for severe deep-water environment.

In summary, the design scheme of sandglass-type floating body in this paper is effective and valid, which can take the maximum peak of heave motion RAO away from the concentration zone of wave energy. Thus the new sandglass-type floating body based on the design scheme can significantly improve the performance (heave motion, pitch motion, stability, etc.), and thus can be applied in deepwater oil and gas exploitation as an efficient engineering platform. Furthermore, this paper tentatively introduces the control and optimization of hydrodynamic performance into the shape design of floating body, which can form a more scientific and reasonable design guideline and scheme to provide the reference and experience for the design of other ocean floating structures.

Acknowledgment

The authors are grateful to all organizations that funded the research in this paper, which was financially supported by the National Innovation Team Foundation under grant no. 50921001 (China), the National Natural Science Foundation of China (Grant No. 11202047), the Scientific Research Foundation for Introduction of Talent under grant no. DUT13RC(3)46 (China) and Natural Science Foundation of Liaoning Province under grant no. 2015020157 (China).

References

[1] Banerjee PK, Buttefield R. Boundary element methods in engineering science. London: McGraw Hill; 1981.
[2] Dittrick P. OTC: petrobras emphasizes safety in FPSO design, operation in gulf. Oil Gas J 2013;111(5):22–3.
[3] Faltinsen OM. Sea loads on ships and offshore structures. UK: Cambridge University Press; 1990.
[4] Fontaine E, Orsero P, Ledoux A, et al. Reliability analysis and response based design of a moored FPSO in West Africa. Struct Saf 2013;41(1):82–96.
[5] Gonçalves RT, Matsumoto FT, Malta EB, et al. Evolution of the MPSO (monocolumn production, storage and offloading system). Mar Syst Ocean Technol 2009;5(1):43–51.
[6] Gonçalves RT, Matsumoto FT, Malta EB, et al. Conceptual design of monocolumn production and storage with dry tree capability. J Offshore Mech Arct Eng Trans ASME 2010;132(1):1–12.
[7] Gonçalves RT, Rosetti GF, Fujarra ALC, et al. Experimental comparative study on vortex-induced motion (VIM) of a monocolumn platform. J Offshore Mech Arct Eng Trans ASME 2012;134(1):1–15.
[8] Hooft JP. Advanced dynamics of marine structure. USA: John Wiley & Sons; 1982. p. 86–9.
[9] Huang Y, Wang WH, Yao YX, et al. Sandglass-type floating structure in ocean engineering. ZL 201220526277.4. 2013.
[10] Huang Y, Wang WH, Yao YX, et al. New FPSO with docking truncated cone shape. ZL 201220526712.3. 2013.
[11] Huang Y, Wang WH, Yao YX, et al. New FPSO with docking octagonal pyramid. ZL 201220526306.7. 2013.
[12] Huang Y, Wang WH, Yao YX, et al. A control method for floating condition and stability of floating structure during loading and offloading. ZL 201420129373.4. 2015.
[13] Korvin-Kroukovshy BV, Jacobs WR. Pitching and heaving motions of a ship in regular waves. Trans SNAME 1957;65:590–632.

[14] Ma Y, Hu ZQ, Qu Y, et al. Research on the characteristics and fundamental mechanism of a newly discovered phenomenon of a single moored FPSO in the South China Sea. Ocean Eng 2013;59(1):274–84.
[15] Salvesen N, Tuck EO, Faltinsen OM. Ship motions and sea loads. Trans SNAME 1970;78(8):250–87.
[16] Sphaier SH, Torres FGS, Masetti IQ, et al. Monocolumn behavior in waves: experimental analysis. Ocean Eng 2007;34:1724–33.
[17] Wang TY, Feng YX. Advanced development of research on new concept FPSO. Ship Ocean Eng 2011;40(5):184–9.
[18] Wang WH, Yao YX, Ye MS, et al. Research on design scheme and hydrodynamic performance of floating body based on sandglass-type FDPSO. Ships Offshore Struct April 1, 2015:1–11. Article in Press.
[19] Wu JM. Distinguishing feature and existing circumstances of FPSO. Ship Eng 2012;34(2):1–5.
[20] Yao YX, Wang WH, Huang Y. Concept design of a new sandglass-type floating production storage and offloading system. J Shanghai Jiao Tong Univ 2014;48(4):558–64.
[21] Qian K, Wang YY. Analysis of wave load on a semi-submersible platform. China Ocean Eng 2002;16(3):395–406.
[22] Vladimir STS. Statics and dynamics of the ship: theory of buoyancy, stability and launching. United States.: University Press of the Pacific; 1988.
[23] Hoerner SF. Fluid-dynamic Drag: practical information on aerodynamic drag and hydrodynamic resistance [M]. USA: Hoerner Fluid Dynamics; 1965. p. 36–51.